

Molecular dynamics simulations reveal structural insights into inhibitor binding modes and functionality in human Group IIA phospholipase A(2)

Author

Kim, Ryung Rae, Malde, Alpeshkumar K, Nematollahi, Alireza, Scott, Kieran F, Church, W Bret

Published

2017

Journal Title

Proteins: Structure Function and Bioinformatics

Version

Accepted Manuscript (AM)

DOI

[10.1002/prot.25235](https://doi.org/10.1002/prot.25235)

Rights statement

© 2017 Wiley Periodicals, Inc. This is the pre-peer reviewed version of the following article: Kim, RR; Malde, AK; Nematollahi, A; Scott, KF; Church, WB, Molecular dynamics simulations reveal structural insights into inhibitor binding modes and functionality in human Group IIA phospholipase A(2), Proteins: Structure Function and Bioinformatics, 2017, 85 (5), pp. 827-842, which has been published in final form at <https://doi.org/10.1002/prot.25235>. This article may be used for non-commercial purposes in accordance with Wiley Terms and Conditions for Use of Self-Archived Versions.

Downloaded from

<http://hdl.handle.net/10072/410678>

Griffith Research Online

<https://research-repository.griffith.edu.au>

**Molecular dynamics simulations reveal structural insights into inhibitor binding modes
and functionality in human group IIA phospholipase A₂**

Ryung Rae Kim¹, Alpeshkumar K. Malde², Alireza Nematollahi¹, Kieran F. Scott^{3,4}
and W. Bret Church^{1,*}

¹Group in Biomolecular Structure and Informatics, Faculty of Pharmacy, The University of
Sydney, Sydney NSW 2006, Australia

²School of Chemistry and Molecular Biosciences, University of Queensland, Brisbane QLD
4072, Australia

³School of Medicine, Western Sydney University, The Ingham Institute for Applied Medical
Research, Liverpool NSW 2170, Australia.

⁴Centre for Oncology Education and Research Translation (CONCERT), The Ingham
Institute for Applied Medical Research, Liverpool NSW 2170, Australia.

*To whom correspondence should be addressed:

e-mail address: bret.church@sydney.edu.au

Postal address: Faculty of Pharmacy A15, The University of Sydney, Sydney NSW 2006,
Australia

Tel.: +61-2-9036-6569

Fax: +61-2-9351-4391

Short title: MD simulations of Group IIA phospholipases A₂

Key words: Group IIA phospholipase A₂, FLSYK inhibitor, binding site, vimentin,
molecular dynamics, protein-protein interaction, docking

*To whom correspondence should be addressed.

This article has been accepted for publication and undergone full peer review but has not been
through the copyediting, typesetting, pagination and proofreading process which may lead to
differences between this version and the Version of Record. Please cite this article as an
'Accepted Article', doi: 10.1002/prot.25235

© 2017 Wiley Periodicals, Inc.

Received: Sep 12, 2016; Revised: Dec 14, 2016; Accepted: Dec 21, 2016

Abstract

Human group IIA phospholipase A₂ (hGIIA) promotes inflammation in immune-mediated pathologies by regulating the arachidonic acid pathway through both catalysis-dependent and -independent mechanisms. The hGIIA crystal structure, both alone and inhibitor-bound, together with structures of closely related snake-venom-derived secreted phospholipase enzymes has been well described. However, differentiation of biological and non-biological contacts and the relevance of structures determined from snake venom enzymes to human enzymes are not clear. We employed molecular dynamics (MD) and docking approaches to understand the binding of inhibitors that selectively or non-selectively block the catalysis-independent mechanism of hGIIA. Our results indicate that hGIIA behaves as a monomer in the solution environment rather than a dimer arrangement that is in the asymmetric unit of some crystal structures. The binding mode of a non-selective inhibitor, KH064, was validated by a combination of the experimental electron density and MD simulations. The binding mode of the selective pentapeptide inhibitor FLSYK to hGIIA was stipulated to be different to that of the snake venom phospholipases A₂ of *Daboia russelli pulchella* (svPLA₂). Our data suggest the application of molecular dynamics approaches to crystal structure data is beneficial in evaluating the robustness of conclusions drawn based on crystal structure data alone.

Introduction

Secreted phospholipases A₂ (sPLA₂s) are members of a superfamily of esterases that catalyze the hydrolysis of the ester bond at the *sn*-2 position of glycerophospholipids to release free fatty acids such as arachidonic acid, and lysophospholipids. These are relatively small proteins and have a low molecular weight, ranging from 13 to 19 kDa and possess at least 6 highly conserved disulfide bonds, a catalytic dyad featuring His and Asp residues and a calcium binding loop (Xxx-Cys-Gly-Xxx-Gly-Gly).¹ In order for sPLA₂s to access their

cellular substrate, they must firstly interact with the phospholipid bilayer using a functional binding site called an interfacial binding face which is composed of N-terminal α -helical residues and other hydrophobic residues in proximity that together form a relatively planar surface (**Fig. 1**)^{2,3}. These residues also form an opening where a single phospholipid molecule can enter and penetrate through to the active site cavity where the catalytic dyad is present

Human group IIA (hGIIA, Uniprot accession code P14555), was among the first mammalian subtypes of sPLA₂ characterized. It was originally purified from the synovial fluid of patients with rheumatoid arthritis.⁴⁻⁷ Due to the ability of these enzymes to provide substrates to cyclooxygenases (COXs) and lipoxygenases (LOXs) in the arachidonic acid pathway, hGIIA is implicated in pathology of specific diseases with an inflammatory component.

Although the overall activity of hGIIA in healthy individuals is relatively low and confined to glandular secretions, in inflammatory diseases such as rheumatoid arthritis⁸, acute coronary syndrome,^{9,10} sepsis,¹¹ cancer,^{12,13} acute pancreatitis¹⁴ and asthma,¹⁵ marked induction of the enzyme in the plasma is observed, which is also correlated with the disease severity. In the case of rheumatoid arthritis, its concentration in plasma can rise up to 8-fold over normal.¹⁶

Snake venom sPLA₂s, on the other hand, can exert more diverse physiological effects than the mammalian sPLA₂ types, including neurotoxicity, myotoxicity, cardiotoxicity, platelet aggregation and anticoagulant effects, in spite of having a high amino acid sequence identity in comparisons that range from 30 to 60% to hGIIA.^{17,18} In the case of sPLA₂ purified from the venom of *Daboia russelli pulchella* (VRV-PL-VIIIa, svPLA₂, Uniprot accession code P59071), a 49% identity to hGIIA is seen (**Fig. S1**).

In comparison with other human sPLA₂ subgroups, such as Group V and Group X, or other mammalian group IIA sPLA₂s, hGIIA exhibits lower catalytic activity towards the zwitterionic phosphatidylcholine (PC) bilayer substrates.¹⁹⁻²¹ The origin of this would

appear to be associated with the unusually large number of basic residues, giving more selectivity towards anionic charged glycerophospholipids.¹ It is also partially explained by the absence of a tryptophan residue on the interfacial binding surface that is present in a subset of snake venom sPLA₂s, such as Trp20 in the *Naja Naja* venoms (Uniprot accession code P15445) or other subgroups of human sPLA₂, such as found in the group V (Uniprot accession code P39877) as Trp30. The amphiphilic indole moiety of the tryptophan would promote the penetration of the enzyme into the lipid interface of the phospholipid bilayer, thereby allowing the access of the substrate into the catalytic active site. In fact, the V3W mutation introduced into hGIIA enhanced the activity towards unilamellar PC vesicles by over 250-fold.²² Furthermore, in a study using the H₄₇Q mutant of hGIIA, which only exhibits 1% of the residual catalytic activity compared to the native enzyme, it was demonstrated that it retained its ability to promote prostaglandin E₂ (PGE₂) production and COX-2 expression in fibroblast-like synoviocytes (FLS) obtained from patients with rheumatoid arthritis, in the presence of tumor necrosis factor α (TNF α).²³ Taken together, these observations suggest that the catalytic activity of hGIIA alone does not sufficiently explain its role in the inflammatory pathway. hGIIA has an ability to activate several signaling pathways through direct interaction with another protein and a few candidates such as heparin sulfate proteoglycan (HSPG),²⁴⁻²⁶ integrins α v β 3, α 4 β 1 and α 5 β 1^{27,28} and vimentin²⁹ have been suggested as binding partners. Similarly for the snake venom sPLA₂s, it is suggested that while the catalytic activity is mainly responsible for the digestion of lipids in prey, other toxicological effects have been attributed to the interaction with another protein target via a separate binding site distinct from the substrate binding site.^{18,30}

It has previously been demonstrated that the catalysis-dependent and -independent actions of hGIIA are pharmacologically distinguishable and that cyclic analogues of the pentapeptide FLSYK (Phe-Leu-Ser-Tyr-Lys) were identified to be a unique class of inhibitors that

selectively block the interaction between hGIIA and vimentin.²⁹ This results in the inhibition of PGE₂ production, whilst being only a very weak inhibitor of diheptanoyl PC (DHPC) hydrolysis. Interestingly FLSYK is an endogenous sequence, originally found from the tryptic digestion of the hGIIA itself.³¹ From molecular docking studies, which predicted a close association between the N- and C-termini of the pentapeptide upon binding to hGIIA, cyclic pentapeptide analogues of the FLSYK, including cyclic 2-Nal-Leu-Ser-2-Nal-Arg (c2), were developed which had improved the inhibitory potency by 5 to 50 fold and this enhancement in the potency of inhibition of hydrolysis can be explained by the increased affinity to hGIIA.³² These observations are also consistent with the increased inhibitory action on PGE₂ release from fibroblast-like synoviocytes (FLS), which results from prevention of the interaction between hGIIA and vimentin.²⁹

Currently there are two X-ray crystal structures of the complex of sPLA₂ and the FLSYK inhibitor,^{33,34} which in both cases are the svPLA₂ subtype of the protein. The overall conformation of FLSYK in the two crystal structures and data from computational modelling³² are in conflict, and provide no consistent model of FLSYK binding to hGIIA.

Importantly, there are two X-ray crystal structures of hGIIA in complex with KH064 ((S)-5-(4-Benzyloxy-Phenyl)-4-(7-Phenyl-Heptanoilamino)-Pentanoic acid, KH064),³⁵ an inhibitor that blocks both the catalysis-dependent and -independent action of hGIIA,²⁹ but they show differences in conformations. A series of molecular dynamics (MD) simulations studies have been performed to understand the structure and binding of the ligands to svPLA₂ and hGIIA.

The aim is to resolve the apparent inconsistencies in the binding of ligand in hGIIA and svPLA₂.

Methods

Preparation of molecules and parameters

The initial structures of hGIIA complexed with the ligand KH064 were taken from the PDB entries 1J1A³⁵ and 3U8H.²⁹ The crystal structure 1J1A has two alternate binding modes of KH064 that occur in a 50:50 occupancy ratio, while 3U8H only has a single binding mode differing from the other two. Each of these three binding modes of KH064 was independently subjected to MD simulations and analysis. The topologies of the ligand molecules KH064 were generated using the 'Automated Topology Builder' (ATB) and are available from the ATB repository version 2.2 (<https://atb.uq.edu.au>).³⁶

The ligand-free hGIIA was prepared from 3U8I,²⁹ which was chosen as it has been determined at 1.1 Å resolution, the highest of all hGIIA structures available at the PDB. However, as 3U8I has the inhibitor *p*-bromophenacyl bromide (BPB) covalently bound to the His47, in order to prepare the native ligand-free protein this non-standard residue was modified to the native standard histidine residue, and the inhibitor eliminated.

The svPLA₂:FLSYK used in the study was the 1JQ9³³ structure, which at 1.8 Å is the highest resolution. The FLSYK inhibitor used in the study was prepared as a non-modified peptide with charges allocated at the physiological pH. For initial positioning of the FLSYK ligand in hGIIA, hGIIA structure was superimposed on the svPLA₂:FLSYK complex using the pair_fit function of PyMol 1.6 (Schrödinger, LLC), so that the relative position of the ligand to the protein is transferred to hGIIA after removal of the svPLA₂ structure.

The MD simulations in a solution environment were performed in a truncated octahedral box with ~23500 simple point charge (SPC) water molecules.³⁷ The configuration of the solvent was relaxed by performing a steepest descent minimization. The system was then further equilibrated by performing a 200 ps MD simulation, with the heavy atoms of the protein positionally restrained, before a series of unrestrained MD simulations were commenced.

The simulation of 1J1A and 3U8H in their crystal environment was performed by creating crystal unit cell models. The crystal structures 1J1A and 3U8H are isomorphous in the $P3_1$ space group and contain two protein molecules, each with a single KH064 molecule, in the asymmetric unit. A unit cell comprises three asymmetric units, which includes a total of 6 protein chains and 6 ligands. A unit cell for 1J1A (both binding modes) and 3U8H structure was constructed using the CCP4 program.³⁸ All component molecules as deposited in the PDB file including the crystal solvent (water) and Ca^{2+} ions were used in crystal MD simulations. The crystal solvent contents were 55.0% for 1J1A and 57.5% for 3U8H. Sodium and chloride ions were added and provided an overall neutral charge using the default protocol. This process added 10 sodium and 142 chloride ions into each unit cell of both binding modes of 1J1A, while for the unit cell of 3U8H structure 10 sodium and 130 chloride ions were added. Crystal unit cells were simulated under a triclinic periodic boundary condition.

Molecular dynamics

All MD simulations were performed using the GROMOS11 simulation package^{39,40} in conjunction with the GROMOS 54A7 force field.⁴¹ All the simulations were performed at constant temperature (298 K) and pressure (1 atm). This was achieved using a Berendsen thermostat with a coupling time of 0.1 ps and a Berendsen barostat with a coupling time of 0.5 ps.⁴² The isothermal compressibility was set to 4.575×10^{-4} kJ/mol/nm³. Non-bonded interactions were calculated using a twin-range cutoff. Interactions within the short-range cutoff of 0.8 nm were updated every time step. Interactions within the longer-range cutoff of 1.4 nm were updated every 5 time steps together with the pairlist. To correct for the truncation of electrostatic interactions beyond the 1.4 nm long-range cutoff a reaction field correction was applied using an effective dielectric (ϵ) of 61. The equations of motion were integrated using the leapfrog scheme with a 2 fs time step. Initial velocities at a given

temperature were taken from a Maxwell-Boltzmann distribution. The lengths of all bonds were constrained to ideal values using the SHAKE algorithm with a geometric tolerance of 0.0001.⁴³ The list of MD simulations performed is summarized in **Table 1**.

Docking studies

Docking was conducted with Glide as part of the Schrödinger Maestro software suite 10.2. Chain A of the hGIIA X-ray crystal structure 3U8H was imported and all hetero atoms that are not part of the polypeptide other than the two calcium ions were removed. Using the Protein Preparation module, the protein was assigned with hydrogens, charges and correct bond orders. Missing atoms on Arg123 residues were automatically built and for residues with alternate positions, only the positions with higher average occupancy were used. The grid was generated at the centroid of the protein, with the size of 36 Å × 36 Å × 36 Å, which encompasses the surface of the binding area near the N-terminus. FLSYK and KH064 ligand structures were processed by the Ligand Preparation module as per default settings under the OPLS 2005 force field, except ligands were ionized by generating possible states at pH 7.4 using Epik. The generated ligands were docked with Glide extra precision setting (XP mode) also using the flexible ligand option to allow for all possible torsional variations.

Data analysis

The coordinates, structure factors and electron density maps for 1J1A and 3U8H were obtained from the PDB and EDS (electron density server; <http://eds.bmc.uu.se/eds>) and the atom replacement of KH064 in all three binding modes were examined from difference density maps (2Fo-Fc and Fo-Fc) using PyMOL (Schrödinger, LLC). PyMOL was also used for other calculations such as the distance between atomic coordinates and the centroid of a set of atoms.

The 'Protein interfaces, surfaces and assemblies' service at the European Bioinformatics Institute (PISA, http://www.ebi.ac.uk/pdbe/prot_int/pistart.html)⁴⁴ was used for analyzing the interfaces between protein chains with another protein chain, a ligand or a protein chain and a ligand. The area of interfaces involved, the solvation free energy gain and the residues involved in the formation of interface were determined in the analysis. The MolProbity server (<http://molprobity.biochem.duke.edu/index.php>)⁴⁵ was used to assess the quality of protein and peptide structures by inspecting the overall clash score, Ramachandran plot, rotamers, bond angles and bond lengths.

All MD trajectories were analysed using the Gromos++ set of programs. The backbone root mean square positional deviation (RMSD) of residues within well-defined regions of secondary structure (α -helices and β -sheets) between all possible pairs of structures were determined. The time series of torsional dihedral angles for all 3 rotatable bonds of KH064 molecule (-Ar-O-; -O-CH₂-; -CH₂-Ar-) were calculated across the trajectories.

Results

Validation of hGIIA:KH064 complex structures

The atom placement and electron densities of all three binding modes of KH064 in hGIIA crystal structures were analyzed and compared. From the inspection of differential electron density maps, it is clear that in both conformers of 1J1A that the atoms are less appropriately placed in comparison to 3U8H, and particularly around the benzyl ether moiety, as clearly displayed in the Fo-Fc map (**Fig. 2**).

In all three binding modes in the crystal structures, there are two chains of the protein in close contact with each other on the interfacial binding face of the protein, where substrates access and enter the active site (**Fig. 3 A, D, G**). This forms part of the larger interface between the

two protein chains in the asymmetric unit deposited in the PDB. After 1 ns of MD simulations in the solution environment, the separation of the monomer chains is observed in all these calculations, with minimal contact between them (**Fig. 3 B, C, E, F, H, I**). In case of the two binding modes of 1J1A, complete separation of monomer chains occurs. In the MD runs of 3U8H, the monomer chains are held in close proximity only by the weak π -stacking force between the phenyl rings of each of KH064 ligand, which was not seen for 1J1A, while there were no interactions between the macromolecule chains. When compared to the results of MD simulations in the crystal environment, this suggests that the apparent dimer structure of the asymmetric unit in the crystal structure and its interface is stabilized only by the crystal packing forces. The KH064 ligand remained within the N-terminal binding site of the protein throughout in all six simulations although it displayed high flexibility.

For the MD simulations on all three binding modes of KH064 to hGIIA in the crystal environment, the conformation found in 3U8D displayed evidence for less fluctuation in comparison to both KH064 structures of 1J1A. This is consistent with the RMSD of the six KH064 ligands in a unit cell, as the RMSD plot shows that the conformation of KH064 ligands in 3U8H were remained more persistent and formed a more steady plateau state in comparison to the other two (**Fig. S2**). The difference in structural fluctuations is most pronounced in the analysis of the dihedral angle between CH_2 and the aromatic ring of the ligand (**Fig. 4**). In the crystal structure, the dihedral angle around $-\text{CH}_2\text{-Ar-}$ (of the benzyl ether group) of the ligand is -90° for the first binding mode of 1J1A, 165° for the second binding mode of 1J1A and -100° for 3U8H. While both 1J1A ligand conformations demonstrate fluctuations of the dihedral angle right through -180° to 180° over the course of MD simulations, the dihedral angle in 3U8H remains relatively steady around -100° with significantly fewer fluctuations. The analysis of RMSD and dihedral angles data together are convincing that the ligand conformation found in 3U8H is relatively more stable than the

other two structures. Although the different position of the benzyl ether group of the KH064 ligand displayed a significantly different level of fluctuations of the dihedral angle around -CH₂-Ar- between the three binding modes, it is notable that the phenyl heptadyl group occupies the same region of the protein in all three binding modes. This region is adjacent to the N-terminal α -helix, at the entrance leading to the active site.

Prediction of stoichiometry of ligand-free hGIIA in a solution environment

Both chains of ligand-free hGIIA prepared from 3U8I were subjected to MD simulations in the solution environment, which was conducted in duplicate runs. At time 0 (**Fig. 5 A**), which represents the protein conformation of the X-ray crystal structure, the two protein chains form a dimeric interface between 15 residues of each chain, namely Asn1-Val3, His6, Arg7, Lys10, Glu16, Ala18, Leu19, Phe23, Val30, Lys62, Phe63, Tyr111 and Ser113, with a size of 582.8 Å², which represents a gain in solvation free energy of -13.8 kcal/mol. Within 1 ns of the MD simulation, the two chains of the proteins were starting to separate and by 10 ns of the simulation, each chain was completely divorced from the other in both MD runs (**Fig. 5 B and C**). This is also consistent with the results from the MD simulation of the hGIIA:KH064 dimeric complex described above. In the presence of the KH064 ligand, the two chains were held only weakly by the π -stacking forces of the KH064 ligand, but in this simulation, complete separation was observed. The formation of the dimeric interface observed in the crystal structure, although energetically favorable with a negative solvation free energy value, seems to be a phenomenon that only occurs in this crystal environment and is also unfavorable in the solution environment.

Binding of FLSYK pentapeptide in hGIIA and svPLA₂

In the crystal structure of FLSYK-bound svPLA₂ 1JQ9, the ligand FLSYK directly interacts with the chain A of the protein by forming an interface area of 542.7 Å² with a gain in

solvation free energy of -6.7 kcal/mol while having minimal interactions with chain B of the protein. MD simulation calculations were performed in parallel for both the complexes of the svPLA₂ dimer (chain A and B):FLSYK and the svPLA₂ monomer (chain A):FLSYK in the solution environment. The dimer:FLSYK MD simulation revealed that the stability of the dimeric structure is retained in the solution environment as shown in the minimal changes of the backbone RMSD (see **Fig. S3**, and also **Fig. S4** for RMSF plots). However, the ligand FLSYK, adopted alternate conformations and novel interactions with chain B of the protein (**Fig. 6**). There was no global conformational change of the protein in either of the runs of MD simulation of the monomer:FLSYK complex, as the backbone RMSD remained within a range of 0.2 to 0.4 nm (**Fig. S5**). In the monomer:FLSYK MD simulation the ligand migrated away from the known binding site at the entrance to the active site and adopted alternative conformations as seen in the large RMSD of the backbone of the FLSYK attaining over 0.8 nm (**Fig. 7 A**). Further analysis confirms that the ligand is no longer occupying the binding site at the time when the large RMSD is observed. In the other run, the FLSYK stayed within the binding site, and the RMSD remained within the 0.2 to 0.5 nm range over throughout the first 20 ns of the simulation.

We performed an MD simulation to examine the interaction of the both the hGIIA monomer and dimer structures and FLSYK. In both of the hGIIA dimer:FLSYK complex simulations performed, the chain B was completely separated from chain A after 1 ns (**Fig. S6**), and therefore it was decided only a further test of the hGIIA monomer:FLSYK complex was required. The hGIIA monomer:FLSYK complex was found to be highly unstable, as supported by the large RMSD in both runs of MD simulations, reaching over 2 nm in one of the runs (**Fig. S7**). The orientation of FLSYK in 1JQ9 cannot be maintained as might be predicted from a simple superimposition with the hGIIA structure. When the hGIIA structure is simply overlaid with the chain A of 1JQ9, the FLSYK ligand had a steric hindrance with

hGIIA at His6 (**Fig. S8**), and therefore it was considered necessary to relax the macromolecule before we could proceed with MD simulation. The results indicate that the binding mode of FLSYK to the monomeric hGIIA is significantly different from that to the monomeric svPLA₂, and therefore 1JQ9 does not provide any useful model of how the FLSYK binds in a hGIIA:FLSYK complex, any more than that the binding would be at or near the active site entrance.

Docking ligands to the hGIIA structure

In order to further consider the requirements of FLSYK binding to hGIIA, docking of the KH064 ligand on the chain A of 3U8H structure with Glide was performed. A total of four poses were generated, which are of high similarity to the conformation of KH064 found in the X-ray crystal structure 3U8H (**Fig. S9**). The RMSD of the docked ligands in comparison to the KH064 found in the 3U8H structure ranged from 1.5 to 1.7 Å across all four results.

Although the positions of the phenyl groups and the dihedral angles of the carbon chains are not identical to those in the crystal structures, overall the contacts the ligand make to the surrounding hydrophobic groups and the formation hydrogen bonds are reproduced by the docking simulation to a high level of similarity.

In the docking of FLSYK to the chain A of 3U8H, the top six poses had docking scores less than -9.0. These were of -9.93, -9.80, -9.69, -9.62, -9.55 and -9.35, where the increasing negativity indicates more favorable interaction in the docking calculations. The top six docking poses display the ligands occupying a similar region of the protein within the N-terminal binding site, but are significantly different to the region FLSYK binds to on svPLA₂ in the 1JQ9 X-ray crystal structure (**Fig. 8**). The RMSDs of the second to sixth scoring conformations in comparison to the top scoring pose are 2.2, 1.5, 1.6, 2.1 and 2.2 Å respectively, and 1.6, 1.0, 1.3, 1.8 and 1.5 Å respectively, when backbone atoms only were

considered. In all six results, the leucine sidechain of the ligand formed hydrophobic interactions with the surrounding Leu2 Phe5 and Val30 residues of hGIIA while hydrogen bonds formed were between one of the hydrogen atoms of the N-terminal amino group of the ligand and the N^{δ1} atom of His47, and the backbone oxygen atom in the phenylalanine of the ligand and the hydrogen on the backbone nitrogen of Gly29.

Discussion

X-ray crystallography remains an indispensable tool in the structural biology, and especially for deciphering how a ligand binds to its target protein. However, the accuracy and utility of structural information that can be deduced from the X-ray crystallography depends on multiple factors including, most evidently, the resolution. The general limitations in the descriptions of the binding mode, orientation and conformation of small non-covalently bound organic ligand molecules in crystallography do exist and are well-documented.⁴⁶ In addition, it may also be difficult in some cases to observe conclusive electron density evidence in the supposed binding region, where it only partially exists or is minimal. In the extreme situation the crystallographic approval is intractable, even when some clear electron density exists which is unexplained by the protein atoms and solvent alone. Some relatively ambiguous binding conformations have been well described in the literature,⁴⁷ but in general active sites in proteins are more ordered than elsewhere. Also, and more especially in the case of ligands of extended length or size, crystallography can determine there is more ordered binding in one region relative to another. Focused scrutiny of the ligands, and the electron density in the vicinity, can remove most ambiguity, though assessments of the interpretations are sometimes continuously made, including after deposition of coordinates has been made with the databank.⁴⁸ The trials and tribulations of placing ligands in protein crystal structures have been reviewed in the literature from a number of perspectives.^{47,49-52} There is also evidence that the details of the crystal, and the manner in which the ligand is introduced can

affect the mode of binding, representing strong evidence that there is no complete guarantee that publically released structural coordinates are representative for the biologically active species. Very recently a report has been made that the existence of polyethylenes as precipitant or cryoprotectants in crystals can influence the location observed of ligands,⁵³ and although there are no polyethylenes in any crystal structures used in this study, it serves as a reminder that variants of the protein environment could have an effect on the location of the ligand. We have examined the ligand binding for a number of Group IIA sPLA₂:ligand complexes for which there are crystal structures available with high resolution (equal or less than 2.3 Å), for the purposes of a better understanding of the inhibitory mechanisms available for hGIIA.

It has been established that hGIIA can provide a dual function, exerting its actions through either catalysis-dependent or -independent mechanisms.²³ However, little is known about how the catalysis-independent mechanism relates to the structural aspects of the protein as only relatively subtle conformational changes have been described.²⁹ Allosteric inhibition must be considered for the inhibition of the catalysis-independent action, as it may not involve a global conformational change of hGIIA because the catalytic machinery activity of the protein would need to remain unaffected. The protein very conceivably has at least two distinguishable ligand binding sites that each play an important role for the mechanism of action, or more simply the inhibition is achieved at a single binding site involving a subtle local conformational change, which could be the case especially for the non-selective inhibitors.

In the work, we used MD to assess the stability of the structure model, for instance in the area of ligand binding by considering the fluctuations of the ligand. Checking the atom placement in the electron density is the primary method of assessing the validity of the ligand binding in crystallography, but MD simulations have been used as an additional structural validation

tool, exploring the assumption that the conformation found in the crystal structure is the most stable. Models with less fluctuation during the MD simulation, and less change in RMSD and dihedral angles occupy a more stable conformation.

In the case of the two models of the hGIIA:KH064 complex in 1J1A, inappropriate placement of atoms seemed to have occurred as observed from the inspection of the electron density maps. To determine whether a conformation of KH064 is more favorable, structural validations of all the hGIIA:KH064 complexes were performed using MD simulations. The MD simulation results for the hGIIA:KH064 complexes indicated some fluctuation of the ligand in all three models tested, which was within our prior expectations since the KH064 molecule is highly flexible. The MD did support that the KH064 ligand was more stable in the 3U8H simulation than the two 1J1A simulations and is evidence of the appropriateness of the KH064 conformation observed in the 3U8H crystal structure. However, it is possible in cases where multiple conformations may exist, the calculated energy from MD may be similar enough that there is no way to distinguish them. Limitations to MD analysis is seen in such cases, as it is difficult to determine whether multiple conformations exist in the physiological environment as multiple energy troughs may exist in the molecule, or the power of MD technique not being sensitive enough to determine the single lowest energy.

Although the difference in placement of the benzyl ether group of KH064 in each of the hGIIA:KH064 complex structures affected the degree of the fluctuations upon MD simulations significantly, it was observed that the phenyl heptadyl group, which is highly hydrophobic, occupies the N-terminal binding site constantly in all three binding modes of the ligand. **Table 2** displays the χ_1 (C-C α -C β -C γ) dihedral angle of the His6 residue, which is a part of the N-terminal α -helix, of all hGIIA crystal structures available at the PDB. The dihedral angle is within the range of 155.7° to 168.7° for the ligand-free hGIIA structures and 3U8H. The KH064 is an inhibitor selective for the catalytic-dependent mechanism covalently

bound at His47, distant from the N-terminal α -helix. All ligand-bound hGIIA crystal structures have the dihedral angle ranging between 55.0° and 72.2° , including the 3U8D structure which has a LY311727 ligand that is known to non-selectively inhibit both the catalysis-dependent and -independent mechanisms.²⁹ The common feature shared in these crystal structures is that upon the introduction of a ligand at the N-terminal binding site at the entrance to the active site, a local conformational change involving the rotation of His6 around the χ_1 dihedral is induced, which subsequently causes an enlargement of the ligand binding site adjacent to this residue. The space created is then occupied by the hydrophobic or aromatic moiety of the ligand, and is within 4 Å of the C β atom of His6. This has been previously put forward as the general mechanism of action for the inhibition of the catalysis-independent mechanism and more specifically for the interaction between hGIIA and vimentin.²⁹ Although there are two non-selective inhibitors occupying this space, as found in structures 3U8D and 3U8H, we are yet to determine whether the other inhibitors binding to this pocket exhibit such non-selective inhibition. If future experiments could demonstrate that inhibitors selective towards catalysis-independent mechanism use their hydrophobic moiety to occupy this space of hGIIA, this region could be shown to be a significant feature in the interaction with vimentin.

There are 16 X-ray crystal structures of hGIIA published in the PDB, of which eight consist of an asymmetric unit of only a single chain, six structures of two chains and two structures of six chains (**Table 2**). The protein biological unit stoichiometry of hGIIA is listed in the PDB as homodimer for five structures and monomer for eleven. Due to such inconsistencies, and no known previous systematic effort to understand the biologically active species, we examined features relating to functional stoichiometry and how hGIIA might exist in the physiological conditions by performing MD simulations in a solution environment, as an assembly or not.

We have conducted MD simulations of the KH064-bound hGIIA structures in both the crystal and solution environments in order to test the hypothesis that the association observed in the crystal structure is a consequence of the crystal packing effect only, rather than that it exists as a dimer in solution. In the MD simulations the dimer was stable in the crystal environment but the two chains separated in solution. Similarly, the two protein chains separated in the simulations of the ligand-free hGIIA structures in solution. Overall, our study shows that it is unlikely for hGIIA to exist as a dimer in a solution environment or the physiological conditions, although it cannot be unambiguously shown that a dimeric form of hGIIA cannot exist in some environments, and also conceivably in equilibrium with the monomer. The use of the monomeric chain alone can be implied for modelling the interactions of hGIIA, especially for the one that involves vimentin. The binding site of hGIIA where the non-selective inhibitors bind is important for the interaction with vimentin, as interference of this region with the inhibitor led to inhibition of the proinflammatory signal caused by the interaction.²⁹ If hGIIA existed as a dimer under physiological conditions, this region would not have sufficient solvent exposure to allow any interaction with vimentin.

That the biologically active unit only consists of the monomer for hGIIA in the solution environment is perhaps not particularly surprising, as the entrance to the active site near the N-terminus should be exposed to the “exterior” in order for the natural substrate to enter and access the catalytic site. The formation of the interface between the two protein chains observed in some hGIIA crystal structures would completely block the exposure of the entrance to the substrate. In such a dimer form the protein would be anticipated to have a severe handicap to the catalysis. The formation of interfaces found in several hGIIA crystal structures occurs between substantially different residues or areas of the protein, with different interface sizes (**Table S1**). The dimer structures we have used for MD simulations (3U8H and 3U8I) have interface area with favorable solvation energy, and therefore are

highly represented in the experimental structures, although they became unstable upon simulations in solution. The crystallographic data shows the potential for many interfaces in the crystal forms, but a conclusion about favored interactions is not possible.

There is no X-ray crystal structure of the complex between hGIIA and FLSYK pentapeptide or its analogue inhibitors. 1JQ9 represents the structure of a complex between the homodimer of svPLA₂, a structurally similar protein to hGIIA, and the FLSYK ligand, which might be anticipated to serve as an excellent scaffold for modelling the binding of FLSYK to hGIIA.

As earlier calculations established that hGIIA is most likely to exist as a monomer under the physiological conditions, it is reasonable to model the binding of FLSYK to the hGIIA in its monomeric form, rather than as a dimer. Therefore, when we then considered the potential for the svPLA₂:FLSYK complex to be used as a model for the prediction of the hGIIA:FLSYK complex, only the complex of monomeric svPLA₂ and FLSYK was thought to be relevant. However the results showed that the binding of the ligand is stabilized by the interface between the two chains, which implies the necessity of the second chain of svPLA₂. That the FLSYK binding was not stable in monomeric svPLA₂ in one of the MD runs (**Fig. 7 A**) indicates that either FLSYK binding to monomer is not energetically favorable or svPLA₂ and hGIIA behave differently enough that they do not represent analogous situations.

In order to pursue this further, we performed MD simulations appropriate for the study of the interaction of both the monomeric and dimeric hGIIA with FLSYK. Indeed, the results of the MD simulations of the hGIIA dimer:FLSYK complex indicate that the dimeric structure was completely unstable in the presence of the ligand and also the ligand was involved in interactions with only one chain of the protein. This clearly implied that the role of the FLSYK ligand in stabilizing the dimeric structure of the protein would be unique to the svPLA₂ isotype. The results of MD simulations of the hGIIA monomer:FLSYK have

revealed that the 1JQ9 structure does not provide any useful foundation for a prediction of the binding mode of FLSYK in a hGIIA:FLSYK complex, other than that the binding would be at or near the active site entrance.

Docking calculations were employed to produce models of the binding modes of FLSYK on a single chain of hGIIA. Docking does not guarantee to identically reproduce the ligand binding conformations seen in the X-ray crystal structures or the physiological conditions, but rather provide similar poses which are of great value. Using docking calculations on KH064, it was indeed possible to produce ligand placement similar to the one found in the X-ray crystal structure 3U8H, giving an indication of the level of reproducibility possible from the docking calculations. We consider the docking algorithm had performed to expectations.

There are structural differences in the N-terminal binding site between the two sPLA₂s studied in this work, and most notably the glycine in svPLA₂ and histidine in hGIIA at position 6 in the sequences, that are significant in preventing the ligand from binding to hGIIA in the same manner as to svPLA₂. The docking results for FLSYK on hGIIA were significantly different from the FLSYK on svPLA₂ in the 1JQ9 crystal structure. This is in agreement with the MD results for FLSYK with the hGIIA monomer, in so far as the position of the ligand was not as in the 1JQ9 crystal structure because of unstable binding or the adoption of alternative conformations. Considering that the svPLA₂ dimer was stable with FLSYK in the simulations, the specific conformation seen in 1JQ9 may be a situation unique to svPLA₂, and therefore not valid in the case of binding to monomer of hGIIA.

All of the top six docked conformations of FLSYK to hGIIA have two common hydrogen bonds and hydrophobic contacts at the amino acids of the N-terminal side of the ligand.

However it can be seen that the position of the atoms at the C-terminal end, such as the lysine sidechain, is relatively varied between the docking poses. The commonality of the

interactions near the N-terminal end implies the protein residues involved in these interactions are potentially important to the binding and therefore the mechanism of action of FLSYK, but also the observations of the high flexibility on the C-terminal side of the peptide is perhaps unsurprising for such a ligand.

The docking studies produced models of the binding mode of FLSYK to hGIIA, and our top six scoring poses provide our best representation of the physiological situation. Future studies involving X-ray crystallography of the co-crystallization of hGIIA and pentapeptide-based inhibitors, which have been difficult to achieve, would provide an accurate snapshot of the binding mode of the ligand and understandings in what region of the protein is involved in the interaction with another protein.

Conclusions

In this work, the structural aspects of hGIIA function were investigated by studying the binding of varied types of ligands using MD simulations. The work has allowed clarification of some conflicts in the two reported crystal structures in which the inhibitor KH064 is bound to hGIIA. MD simulation served as an important validation tool for determining the correct binding mode of the ligand KH064. The limitations of experiments must be understood and care must be taken when considering the ligand binding modes in the coordinates obtained from the PDB, or the crystallographic results for important ligands are not available. A simple cross-check of the coordinates downloaded from PDB with the electron density data can demonstrate misplacement of ligand atoms despite having accurate placement of protein atoms because the validation criteria for ligand atoms are not as stringent to that of protein atoms. At the extreme the coordinates for a ligand can be chemically invalid or does not reflect the state found in the biological conditions. MD simulation could be used to verify the validity of the ligand binding mode by assessing the degree of stability of binding.

The results here have consistently displayed that hGIIA is favored to exist as a monomer in the biological environment. Intermolecular interactions exist in the hGIIA crystal structures, but may only be stabilized by the total forces of crystal packing, as opposed to being true dimers. In the presence of KH064 ligands, the two monomer chains can be held in proximity by the weak π -stacking forces of the ligand in solution, but the remainder of the protein chain may have no significant interaction with any other.

Our work has served to clarify aspects of the features of the hGIIA that are important for structure-based drug design. More importantly for inhibitors reported to have potential application in disease treatment, the binding of the FLSYK pentapeptide observed with svPLA₂ in the crystal is of little specific consequence for understanding its inhibition of hGIIA. There is great interest in obtaining structural information on the binding of FLSYK to hGIIA, and until more experimental information is available we suggest this work provides the most likely model in which the first three amino acids (FLS) of the pentapeptide are suitably bound at the N-terminal binding site. Altogether, these findings clarify the structural basis of the mechanisms of inhibition of some hGIIA inhibitors, which could be crucial while targeting the interaction of hGIIA with vimentin.

Acknowledgments

This work was supported by an Australian Postgraduate Award (RRK) and a University of Sydney Postgraduate Award (AN). Computational resources for the Molecular Dynamics were provided by the National Computational Infrastructure (NCI, Australia) National Facility (projects m72 and n63). The authors wish to thank members of their respective research groups for a supportive and collegial environment. WBC and KFS are associated with published patents relating to the use of pentapeptides in the treatment of human disease.

References

1. Dennis EA, Cao J, Hsu Y-H, Magrioti V, Kokotos G. Phospholipase A(2) Enzymes: Physical Structure, Biological Function, Disease Implication, Chemical Inhibition, and Therapeutic Intervention. *Chem Rev* 2011;111(10):6130-6185.
2. Jain MK, Gelb MH. Phospholipase A2-catalyzed hydrolysis of vesicles: uses of interfacial catalysis in the scooting mode. *Methods Enzymol* 1991;197:112-125.
3. Winget JM, Pan YH, Bahnson BJ. The interfacial binding surface of phospholipase A2s. *Biochim Biophys Acta* 2006;1761(11):1260-1269.
4. Lai CY, Wada K. Phospholipase A2 from human synovial fluid: purification and structural homology to the placental enzyme. *Biochem Biophys Res Commun* 1988;157(2):488-493.
5. Hara S, Kudo I, Matsuta K, Miyamoto T, Inoue K. Amino acid composition and NH2-terminal amino acid sequence of human phospholipase A2 purified from rheumatoid synovial fluid. *J Biochem* 1988;104(3):326-328.
6. Seilhamer JJ, Pruzanski W, Vadas P, Plant S, Miller JA, Kloss J, Johnson LK. Cloning and recombinant expression of phospholipase A2 present in rheumatoid arthritic synovial fluid. *J Biol Chem* 1989;264(10):5335-5338.
7. Kramer RM, Hession C, Johansen B, Hayes G, McGray P, Chow EP, Tizard R, Pepinsky RB. Structure and properties of a human non-pancreatic phospholipase A2. *J Biol Chem* 1989;264(10):5768-5775.
8. Pruzanski W, Keystone EC, Sternby B, Bombardier C, Snow KM, Vadas P. Serum Phospholipase-A2 Correlates with Disease-Activity in Rheumatoid-Arthritis. *J Rheumatol* 1988;15(9):1351-1355.
9. Hartford M, Wiklund O, Mattsson Hulten L, Perers E, Person A, Herlitz J, Hurt-Camejo E, Karlsson T, Caidahl K. CRP, interleukin-6, secretory phospholipase A2

- group IIA, and intercellular adhesion molecule-1 during the early phase of acute coronary syndromes and long-term follow-up. *Int J Cardiol* 2006;108(1):55-62.
10. Niessen H. Type II secretory phospholipase A2 in cardiovascular disease: a mediator in atherosclerosis and ischemic damage to cardiomyocytes? *Cardiovasc Res* 2003;60(1):68-77.
 11. Endo S, Inada K, Nakae H, Takakuwa T, Yamada Y, Suzuki T, Taniguchi S, Yoshida M, Ogawa M, Teraoka H. Plasma levels of type II phospholipase A(2) and cytokines in patients with sepsis. *Res Commun Mol Pathol Pharmacol* 1995;90(3):413-421.
 12. Menschikowski M, Hagelgans A, Schuler U, Froeschke S, Rosner A, Siegert G. Plasma Levels of Phospholipase A(2)-IIA in Patients with Different Types of Malignancies: Prognosis and Association with Inflammatory and Coagulation Biomarkers. *Pathology & Oncology Research* 2013;19(4):839-846.
 13. Scott KF, Sajinovic M, Hein J, Nixdorf S, Galettis P, Liauw W, de Souza P, Dong Q, Graham GG, Russell PJ. Emerging roles for phospholipase A(2) enzymes in cancer. *Biochimie* 2010;92(6):601-610.
 14. Talvinen KA, Kemppainen EA, Nevalainen TJ. Expression of group II phospholipase A2 in the liver in acute pancreatitis. *Scand J Gastroenterol* 2001;36(11):1217-1221.
 15. Bowton DL, Seeds MC, Fasano MB, Goldsmith B, Bass DA. Phospholipase A(2) and arachidonate increase in bronchoalveolar lavage fluid after inhaled antigen challenge in asthmatics. *Am J Respir Crit Care Med* 1997;155(2):421-425.
 16. Smith GM, Ward RL, McGuigan L, Rajkovic IA, Scott KF. Measurement of human phospholipase A2 in arthritis plasma using a newly developed sandwich ELISA. *Br J Rheumatol* 1992;31(3):175-178.

17. Faure G, Gowda VT, Maroun RC. Characterization of a human coagulation factor Xa-binding site on Viperidae snake venom phospholipases A2 by affinity binding studies and molecular bioinformatics. *BMC Struct Biol* 2007;7:82.
18. Kini RM. Excitement ahead: structure, function and mechanism of snake venom phospholipase A2 enzymes. *Toxicon* 2003;42(8):827-840.
19. Bezzine S, Bollinger JG, Singer AG, Veatch SL, Keller SL, Gelb MH. On the binding preference of human groups IIA and X phospholipases A2 for membranes with anionic phospholipids. *J Biol Chem* 2002;277(50):48523-48534.
20. Han SK, Kim KP, Koduri R, Bittova L, Munoz NM, Leff AR, Wilton DC, Gelb MH, Cho W. Roles of Trp31 in high membrane binding and proinflammatory activity of human group V phospholipase A2. *J Biol Chem* 1999;274(17):11881-11888.
21. Singer AG, Ghomashchi F, Le Calvez C, Bollinger J, Bezzine S, Rouault M, Sadilek M, Nguyen E, Lazdunski M, Lambeau G, Gelb MH. Interfacial kinetic and binding properties of the complete set of human and mouse groups I, II, V, X, and XII secreted phospholipases A2. *J Biol Chem* 2002;277(50):48535-48549.
22. Baker SF, Othman R, Wilton DC. Tryptophan-containing mutant of human (group IIA) secreted phospholipase A(2) has a dramatically increased ability to hydrolyze phosphatidylcholine vesicles and cell membranes. *Biochemistry* 1998;37(38):13203-13211.
23. Bryant KJ, Bidgood MJ, Lei P-W, Taberner M, Salom C, Kumar V, Lee L, Church WB, Courtenay B, Smart BP, Gelb MH, Cahill MA, Graham GG, McNeil HP, Scott KF. A Bifunctional Role for Group IIA Secreted Phospholipase A(2) in Human Rheumatoid Fibroblast-like Synoviocyte Arachidonic Acid Metabolism. *J Biol Chem* 2011;286(4):2492-2503.

24. Beck GC, Yard BA, Schulte J, Haak M, van Ackern K, van der Woude FJ, Kaszkin M. Secreted phospholipases A2 induce the expression of chemokines in microvascular endothelium. *Biochem Biophys Res Commun* 2003;300(3):731-737.
25. Jaulmes A, Janvier B, Andreani M, Raymondjean M. Autocrine and paracrine transcriptional regulation of type IIA secretory phospholipase A2 gene in vascular smooth muscle cells. *Arteriosclerosis Thrombosis and Vascular Biology* 2005;25(6):1161-1167.
26. Boilard E, Bourgoin SG, Bernatchez C, Poubelle PE, Surette ME. Interaction of low molecular weight group IIA phospholipase A(2) with apoptotic human T cells: role of heparan sulfate proteoglycans. *FASEB J* 2003;17(9):1068-1080.
27. Saegusa J, Akakura N, Wu CY, Hoogland C, Ma Z, Lam KS, Liu FT, Takada YK, Takada Y. Pro-inflammatory secretory phospholipase a2 type IIA binds to integrins alpha v beta 3 and alpha 4 beta 1 and induces proliferation of monocytic cells in an integrin-dependent manner. *J Biol Chem* 2008;283(38):26107-26115.
28. Fujita M, Zhu K, Fujita CK, Zhao M, Lam KS, Kurth MJ, Takada YK, Takada Y. Proinflammatory Secreted Phospholipase A2 Type IIA (sPLA-IIA) Induces Integrin Activation through Direct Binding to a Newly Identified Binding Site (Site 2) in Integrins alphavbeta3, alpha4beta1, and alpha5beta1. *J Biol Chem* 2015;290(1):259-271.
29. Lee LK, Bryant KJ, Bouveret R, Lei P-W, Duff AP, Harrop SJ, Huang EP, Harvey RP, Gelb MH, Gray PP, Curmi PM, Cunningham AM, Church WB, Scott KF. Selective Inhibition of Human Group IIA-secreted Phospholipase A(2) (hGIIA) Signaling Reveals Arachidonic Acid Metabolism Is Associated with Colocalization of hGIIA to Vimentin in Rheumatoid Synoviocytes. *J Biol Chem* 2013;288(21):15269-15279.

30. Singh N, Kumar RP, Kumar S, Sharma S, Mir R, Kaur P, Srinivasan A, Singh TP. Simultaneous inhibition of anti-coagulation and inflammation: crystal structure of phospholipase A2 complexed with indomethacin at 1.4 Å resolution reveals the presence of the new common ligand-binding site. *J Mol Recognit* 2009;22(6):437-445.
31. Tseng A, Inglis AS, Scott KF. Native peptide inhibition. Specific inhibition of type II phospholipases A2 by synthetic peptides derived from the primary sequence. *J Biol Chem* 1996;271(39):23992-23998.
32. Church WB, Inglis AS, Tseng A, Duell R, Lei PW, Bryant KJ, Scott KF. A novel approach to the design of inhibitors of human secreted phospholipase A(2) based on native peptide inhibition. *J Biol Chem* 2001;276(35):33156-33164.
33. Chandra V, Jasti J, Kaur P, Dey S, Perbandt M, Srinivasan A, Betzel C, Singh TP. Crystal structure of a complex formed between a snake venom phospholipase A(2) and a potent peptide inhibitor Phe-Leu-Ser-Tyr-Lys at 1.8 Å resolution. *J Biol Chem* 2002;277(43):41079-41085.
34. Kumar M, Kumar S, Vikram G, Singh N, Sinha M, Bhushan A, Kaur P, Srinivasan A, Sharma S, Singh TP. Crystal structure determination of a ternary complex of phospholipase A2 with a pentapeptide FLSYK and Ajmaline at 2.5 Å resolution. Protein Databank, DOI: 102210/pdb3fg5/pdb 2008.
35. Hansford KA, Reid RC, Clark CI, Tyndall JDA, Whitehouse MW, Guthrie T, McGearry RP, Schafer K, Martin JL, Fairlie DP. D-Tyrosine as a chiral precursor to potent inhibitors of human nonpancreatic secretory phospholipase A(2) (IIa) with antiinflammatory activity. *ChemBioChem* 2003;4(2-3):181-185.
36. Malde AK, Zuo L, Breeze M, Stroet M, Poger D, Nair PC, Oostenbrink C, Mark AE. An Automated Force Field Topology Builder (ATB) and Repository: Version 1.0. *J Chem Theory Comput* 2011;7(12):4026-4037.

37. Berendsen HJC, Postma JPM, Gunsteren WF, Hermans J. Interaction Models for Water in Relation to Protein Hydration. In: Pullman B, editor. Intermolecular Forces: Proceedings of the Fourteenth Jerusalem Symposium on Quantum Chemistry and Biochemistry Held in Jerusalem, Israel, April 13–16, 1981. Dordrecht: Springer Netherlands; 1981. p 331-342.
38. Winn MD, Ballard CC, Cowtan KD, Dodson EJ, Emsley P, Evans PR, Keegan RM, Krissinel EB, Leslie AG, McCoy A, McNicholas SJ, Murshudov GN, Pannu NS, Potterton EA, Powell HR, Read RJ, Vagin A, Wilson KS. Overview of the CCP4 suite and current developments. *Acta Crystallogr D Biol Crystallogr* 2011;67(Pt 4):235-242.
39. Schmid N, Christ CD, Christen M, Eichenberger AP, van Gunsteren WF. Architecture, implementation and parallelisation of the GROMOS software for biomolecular simulation. *Comput Phys Commun* 2012;183(4):890-903.
40. Eichenberger AP, Allison JR, Dolenc J, Geerke DP, Horta BA, Meier K, Oostenbrink C, Schmid N, Steiner D, Wang D, van Gunsteren WF. GROMOS++ Software for the Analysis of Biomolecular Simulation Trajectories. *J Chem Theory Comput* 2011;7(10):3379-3390.
41. Schmid N, Eichenberger AP, Choutko A, Riniker S, Winger M, Mark AE, van Gunsteren WF. Definition and testing of the GROMOS force-field versions 54A7 and 54B7. *Eur Biophys J* 2011;40(7):843-856.
42. Berendsen HJC, Postma JPM, van Gunsteren WF, DiNola A, Haak JR. Molecular dynamics with coupling to an external bath. *The Journal of Chemical Physics* 1984;81(8):3684-3690.

43. Ryckaert J-P, Ciccotti G, Berendsen HJ. Numerical integration of the cartesian equations of motion of a system with constraints: molecular dynamics of n-alkanes. *J Comput Phys* 1977;23(3):327-341.
44. Krissinel E, Henrick K. Inference of macromolecular assemblies from crystalline state. *J Mol Biol* 2007;372(3):774-797.
45. Davis IW, Leaver-Fay A, Chen VB, Block JN, Kapral GJ, Wang X, Murray LW, Arendall WB, 3rd, Snoeyink J, Richardson JS, Richardson DC. MolProbity: all-atom contacts and structure validation for proteins and nucleic acids. *Nucleic Acids Res* 2007;35(Web Server issue):W375-383.
46. Malde AK, Mark AE. Challenges in the determination of the binding modes of non-standard ligands in X-ray crystal complexes. *J Comput Aided Mol Des* 2011;25(1):1-12.
47. Davis AM, St-Gallay SA, Kleywegt GJ. Limitations and lessons in the use of X-ray structural information in drug design. *Drug Discov Today* 2008;13(19-20):831-841.
48. Malde AK, Mark AE. Binding and enantiomeric selectivity of threonyl-tRNA synthetase. *J Am Chem Soc* 2009;131(11):3848-3849.
49. Deller MC, Rupp B. Models of protein-ligand crystal structures: trust, but verify. *J Comput Aided Mol Des* 2015;29(9):817-836.
50. Zheng H, Hou J, Zimmerman MD, Wlodawer A, Minor W. The future of crystallography in drug discovery. *Expert Opin Drug Discov* 2014;9(2):125-137.
51. Warren GL, Do TD, Kelley BP, Nicholls A, Warren SD. Essential considerations for using protein-ligand structures in drug discovery. *Drug Discov Today* 2012;17(23-24):1270-1281.

52. Liebeschuetz J, Hennemann J, Olsson T, Groom CR. The good, the bad and the twisted: a survey of ligand geometry in protein crystal structures. *J Comput Aided Mol Des* 2012;26(2):169-183.
53. Dym O, Song W, Felder C, Roth E, Shnyrov V, Ashani Y, Xu Y, Joosten RP, Weiner L, Sussman JL, Silman I. The impact of crystallization conditions on structure-based drug design: A case study on the methylene blue/acetylcholinesterase complex. *Protein Sci* 2016;25(6):1096-1114.

Accepted Article

Figure legends

FIGURE 1 Depiction of hGIIA from PDB accession code 3U8H. Several N-terminal α -helical residues and adjacent hydrophobic residues, labeled and in yellow, constitute the interfacial binding surface that promotes interaction with the aggregated phospholipids.

These residues also form the entrance to the active site cavity where a phospholipid molecule can penetrate. Several hGIIA inhibitors are known to bind to this region, making interaction with some of these residues. Leu2, Val3 and His6 are from the N-terminal α -helix.

FIGURE 2 The ligand found in the first binding mode of 1J1A (A), the second binding mode of 1J1A (B) and the binding mode in 3U8H (C) is shown in stick representation with 2Fo-Fc map contoured at 1 σ on the left and Fo-Fc map contoured at 2 σ on the right. The blue color represents the positive and the red color represents the negative densities. The orientation of the phenyl heptadyl group of the ligand significantly differs between these binding modes and the difference electron density map displays the appropriateness of the atom placement. All three binding modes of KH064 from the two crystal structures, namely 1J1A binding mode #1 (orange), #2 (magenta) and 3U8H (cyan), are superimposed (D). The positions of the ligands in 1J1A binding mode #1 and #2 are identical, except for the position of the phenyl ring. The position of the phenyl rings and the dihedral around -CH₂-Ar- of the benzyl ether group significantly differ between all three binding modes.

FIGURE 3 From left to right, are the crystal structure and snapshots taken at 1 ns after the first MD simulation and the second simulation of hGIIA structures with KH064 ligand. Three crystal structures were subjected to MD simulations, namely 1J1A binding mode #1 (A-C), 1J1A binding mode #2 (D-F) and 3U8H (G-I). The binding mode #1 and #2 refers to the alternative binding mode of the ligand KH064 in the crystal structure 1J1A.

FIGURE 4 Analysis of -CH₂-Ar- dihedral angle for 6 KH064 molecules in the unit cell of 1J1A binding mode #1 (A), binding mode #2 (B) and 3U8H (C).

FIGURE 5 The comparison between the crystal structure (A) and snapshots at 10 ns from MD simulations of ligand-free hGIIA crystal structure 3U8I in duplicate runs (B and C) show complete separation of the two chains occurs in a solution environment. In the first simulation (B), the N-terminal helix displays high mobility through the flip of the adjacent loop between Gly14 and Tyr21.

FIGURE 6 Snapshots at 10 ns of MD simulation of 1JQ9 with both chains of an asymmetric unit and a single FLSYK ligand are shown. Although the FLSYK ligand initially deeply buried in the binding site of the chain A in the crystal structure, it adopted alternate conformations and novel interactions with the chain B were formed at 10 ns of the MD simulation.

FIGURE 7 Backbone RMSD of the FLSYK peptide in the 1JQ9 chain A (monomer) structure in duplicate MD simulations in water (A) show that the binding is not stabilized in MD simulation #2. The snapshot at 20 ns time point for the simulation #2 (D) display the FLSYK ligand adopted an alternative conformation and no longer occupies the original binding site.

FIGURE 8 Conformations of FLSYK with the top six docking scores upon docking on the chain A of 3U8H hGIIA structure are displayed (A). The best scoring docking conformation of FLSYK on hGIIA (cyan) interacts with the region of the protein that is clearly different from the space occupied by the FLSYK ligand found in the 1JQ9 svPLA₂ crystal structure (orange) (B). Also the overall conformations of these two ligands differ significantly. The best scoring docked FLSYK pose forms five hydrogen bonds denoted by yellow dashed lines formed between the ligand and the protein, at positions between a hydrogen of the N-terminus and the Nδ1 of His47, the oxygen of the backbone phenyl and the hydrogen of the backbone nitrogen of Gly29, the oxygen of the backbone serine and the hydrogen of the backbone nitrogen of Gly31, a hydrogen of the amino group of the lysine sidechain and the

carboxyl oxygen of Glu55 sidechain, and an oxygen of the C-terminus and a hydrogen of the amino group of the Lys62 sidechain. Both A and B are in similar orientation to Figure 1.

Accepted Article

Table 1 List of molecular dynamics simulations conducted in the study

PDB ID	Protein	Ligand	Environment	Run time
<i>Validation of hGIIA:KH064 complex structures</i>				
1J1A	Chain A and B of hGIIA	KH064 binding mode #1	Solution	1 ns
1J1A	Chain A and B of hGIIA	KH064 binding mode #2	Solution	1 ns
3U8H	Chain A and B of hGIIA	KH064	Solution	1 ns
1J1A	Unit cell 3 asymmetric units of 6 protein chains of hGIIA	KH064 binding mode #1	Crystal	12 ns
1J1A	Unit cell 3 asymmetric units of 6 protein chains of hGIIA	KH064 binding mode #2	Crystal	12 ns
3U8H	Unit cell 3 asymmetric units of 6 protein chains of hGIIA	KH064	Crystal	7 ns
<i>Prediction of stoichiometry of ligand-free hGIIA in a solution environment</i>				
3U8I	Chain A and B of hGIIA, with ligand unbound His47	None	Solution	10 ns, duplicate runs
<i>Binding of FLSYK pentapeptide in hGIIA and svPLA2</i>				
1JQ9	Chain A and B of svPLA2	FLSYK	Solution	20 ns, duplicate runs
1JQ9	Chain A of svPLA2	FLSYK	Solution	20 ns, duplicate runs
3U8I	Chain A of hGIIA, with ligand unbound His47	FLSYK	Solution	20 ns, duplicate runs
None	None	FLSYK	Solution	50 ns, duplicate runs

Table 2 Selected properties relating to the structure of all PDB entries of hGIIA

PDB	Resolution (Å)	R value	Space group	Number of chains in an asymmetric unit	His6 dihedral angle around χ_1	Ligand in the N-terminal binding site	Hydrophobic group of the ligand within 4 Å of C β of His6
1AYP	2.57	0.214 observed	$P2_1$	6	55.0	Yes	Yes
1BBC	2.2	0.178 observed	$P2_1$	1	168.7	No	N/A
1DB4	2.2	0.256 free 0.226 work	$P6_122$	1	67.2	Yes	Yes
1DB5	2.8	0.240 free 0.196 work	$P6_122$	1	70.4	Yes	Yes
1DCY	2.7	0.269 free 0.218 work	$P6_122$	1	68.3	Yes	Yes
1J1A	2.2	0.258 free 0.227 work	$P3_1$	2	72.2	Yes	Yes
1KQU	2.1	0.240 free 0.209 work	$P6_122$	1	70.2	Yes	Yes
1KVO	2.0	0.273 free 0.201 work	$P2_1$	6	69.4	Yes	Yes
1N28	1.5	0.207 free 0.184 work	$C2$	2	160.2	No	N/A
1N29	2.6	0.320 free 0.242 work	$P6_122$	1	159.8	No	N/A
1POD	2.1	0.193 observed	$P6_122$	1	155.7	No	N/A
1POE	2.1	0.196 observed	$P4_32_12$	2	74.3	Yes	Yes
3U8B	2.3	0.257 free 0.207 work	$P6_122$	1	161.7	No	N/A
3U8D	1.8	0.189 free 0.121 work	$P3_121$	2	71.6	Yes	Yes
3U8H	2.3	0.225 free 0.192 work	$P3_1$	2	70.6	Yes	Yes
3U8I	1.1	0.196 free 0.164 work	$P4_1$	2	164.2	No, but p-bromophenacyl bromide irreversibly bound at His47	N/A

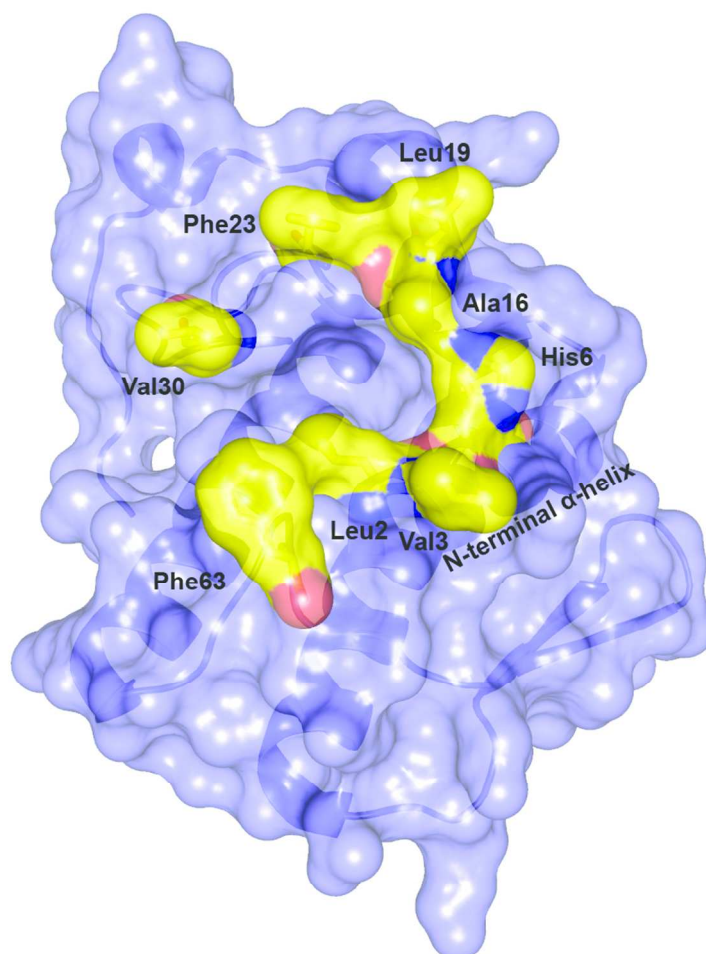
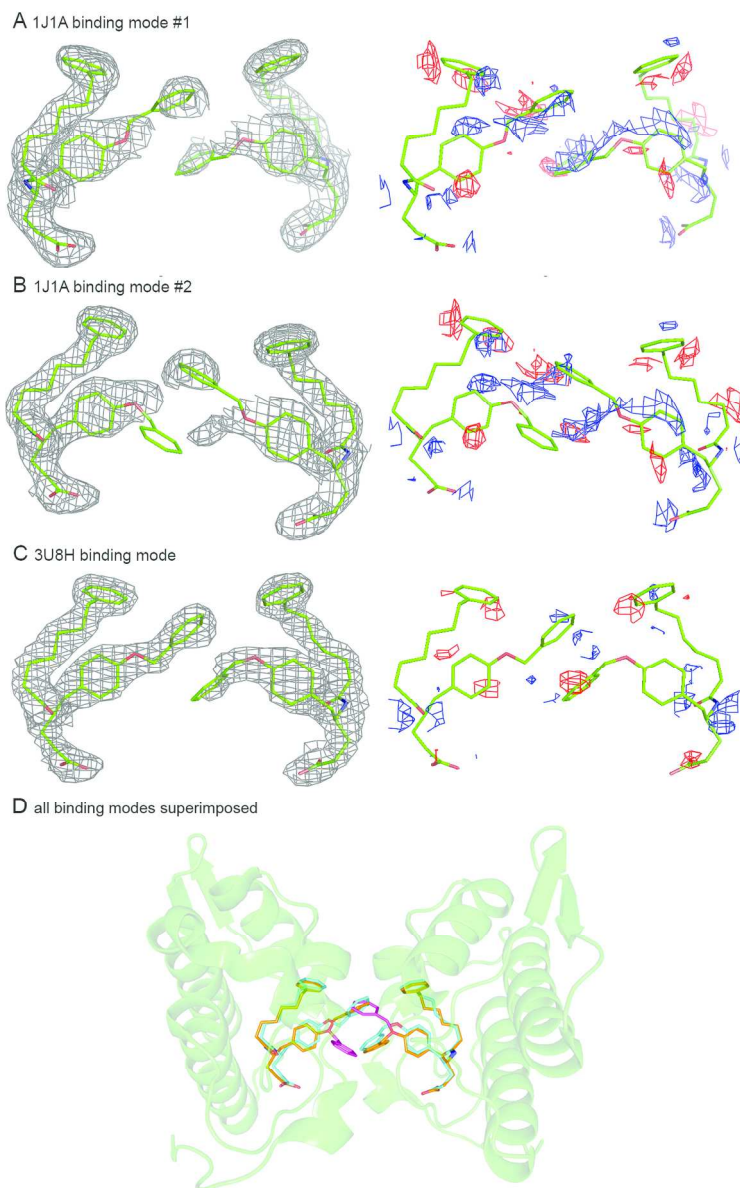


FIGURE 1 Depiction of hGIIA from PDB accession code 3U8H. Several N-terminal α -helical residues and adjacent hydrophobic residues, labeled and in yellow, constitute the interfacial binding surface that promotes interaction with the aggregated phospholipids. These residues also form the entrance to the active site cavity where a phospholipid molecule can penetrate. Several hGIIA inhibitors are known to bind to this region, making interaction with some of these residues. Leu2, Val3 and His6 are from the N-terminal α -helix.

Fig. 1

101x101mm (300 x 300 DPI)

AC



The ligand found in the first binding mode of 1J1A (A), the second binding mode of 1J1A (B) and the binding mode in 3U8H (C) is shown in stick representation with 2Fo-Fc map contoured at 1 σ on the left and Fo-Fc map contoured at 2 σ on the right. The blue color represents the positive and the red color represents the negative densities. The orientation of the phenyl heptadyl group of the ligand significantly differs between these binding modes and the difference electron density map displays the appropriateness of the atom placement. All three binding modes of KH064 from the two crystal structures, namely 1J1A binding mode #1 (orange), #2 (magenta) and 3U8H (cyan), are superimposed (D). The positions of the ligands in 1J1A binding mode #1 and #2 are identical, except for the position of the phenyl ring. The position of the phenyl rings and the dihedral around -CH₂-Ar- of the benzyl ether group significantly differ between all three binding modes.

Fig. 2

120x189mm (300 x 300 DPI)

Accepted Article

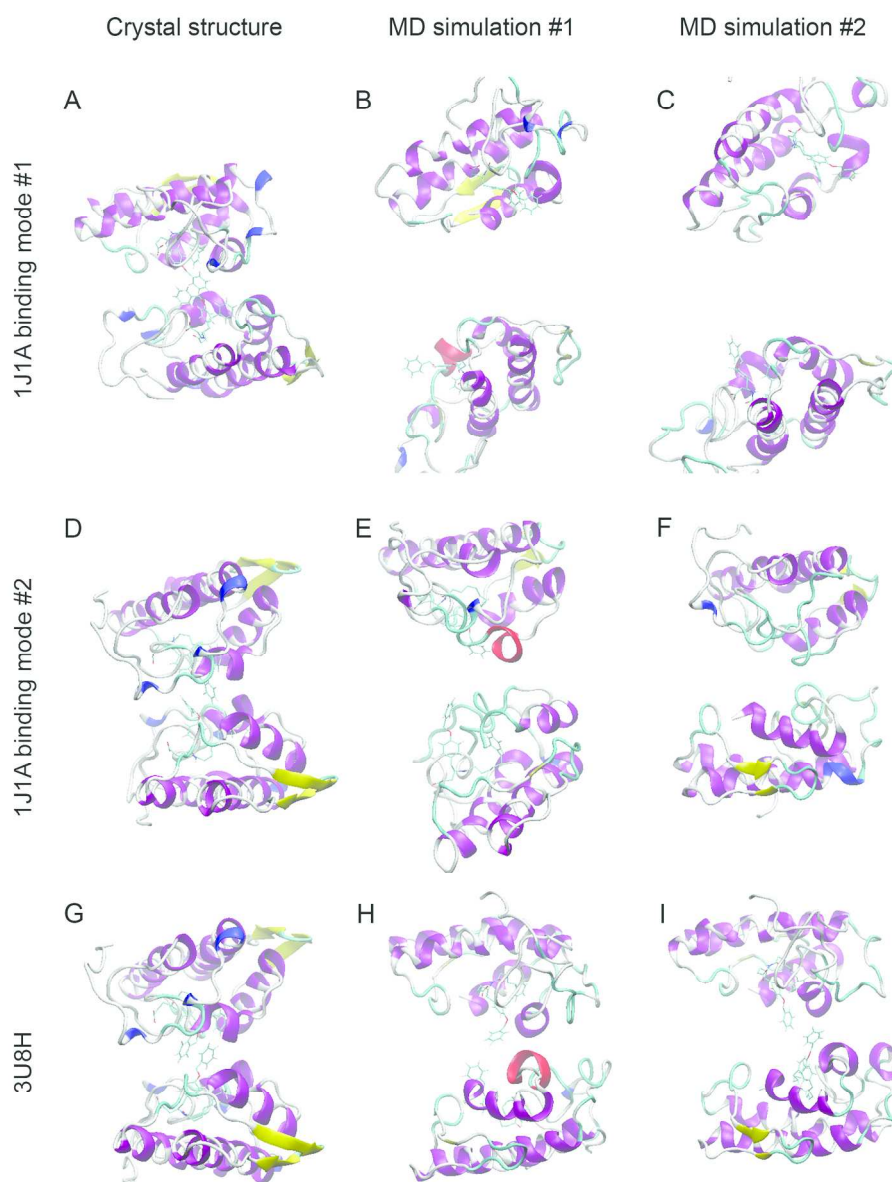


FIGURE 3 From left to right, are the crystal structure and snapshots taken at 1 ns after the first MD simulation and the second simulation of hGIIA structures with KH064 ligand. Three crystal structures were subjected to MD simulations, namely 1J1A binding mode #1 (A-C), 1J1A binding mode #2 (D-F) and 3U8H (G-I). The binding mode #1 and #2 refers to the alternative binding mode of the ligand KH064 in the crystal structure 1J1A.

Fig. 3

177x230mm (300 x 300 DPI)

A

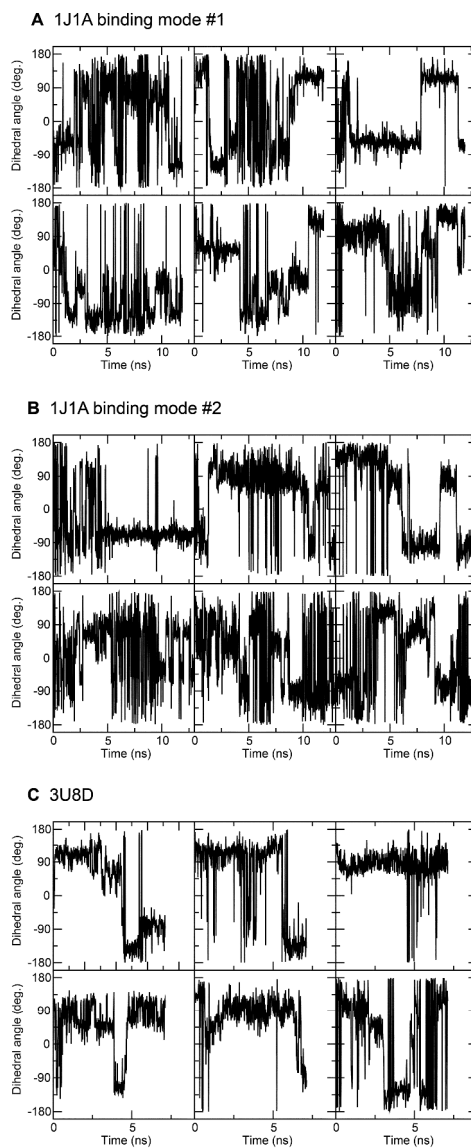


FIGURE 4 Analysis of -CH₂-Ar- dihedral angle for 6 KH064 molecules in the unit cell of 1J1A binding mode #1 (A), binding mode #2 (B) and 3U8H (C).

Fig. 4

189x413mm (600 x 600 DPI)

A

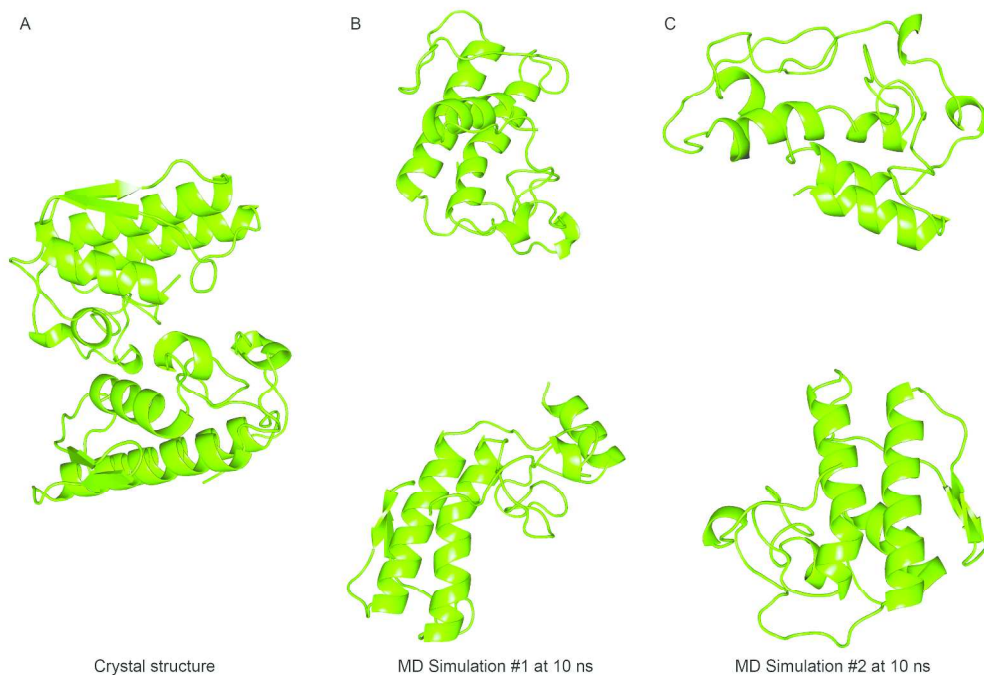


FIGURE 5 The comparison between the crystal structure (A) and snapshots at 10 ns from MD simulations of ligand-free hGIIA crystal structure 3U8I in duplicate runs (B and C) show complete separation of the two chains occurs in a solution environment. In the first simulation (B), the N-terminal helix displays high mobility through the flip of the adjacent loop between Gly14 and Tyr21.

Fig. 5

254x175mm (300 x 300 DPI)

Accepted

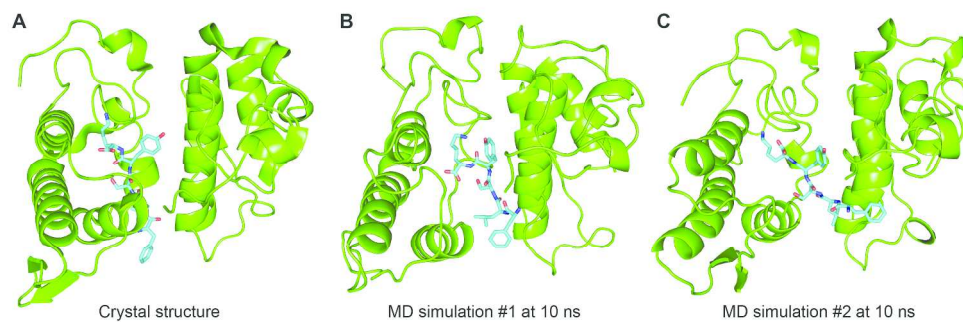


FIGURE 6 Snapshots at 10 ns of MD simulation of 1JQ9 with both chains of an asymmetric unit and a single FLSYK ligand are shown. Although the FLSYK ligand initially deeply buried in the binding site of the chain A in the crystal structure, it adopted alternate conformations and novel interactions with the chain B were formed at 10 ns of the MD simulation.

Fig. 6

254x84mm (300 x 300 DPI)

Accepted

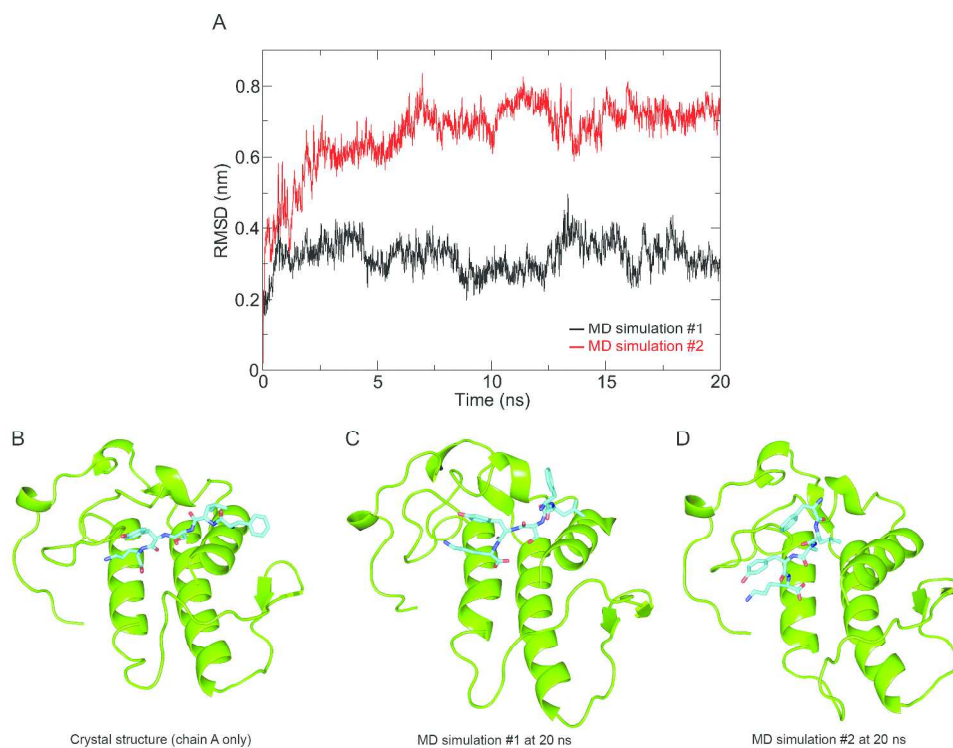
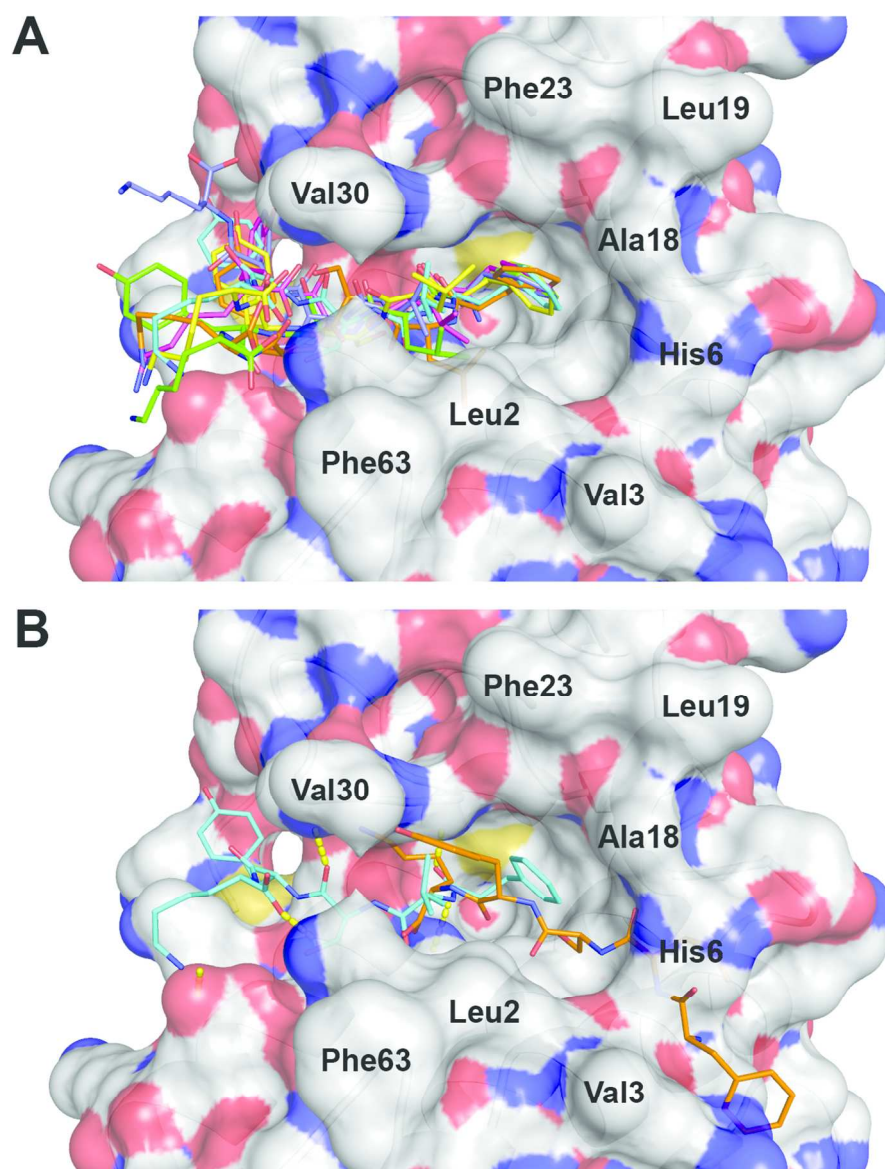


FIGURE 7 Backbone RMSD of the FLSYK peptide in the 1JQ9 chain A (monomer) structure in duplicate MD simulations in water (A) show that the binding is not stabilized in MD simulation #2. The snapshot at 20 ns time point for the simulation #2 (D) display the FLSYK ligand adopted an alternative conformation and no longer occupies the original binding site.

Fig. 7

254x189mm (300 x 300 DPI)

Accep



Caption : FIGURE 8 Conformations of FLSYK with the top six docking scores upon docking on the chain A of 3U8H hGIIA structure are displayed (A). The best scoring docking conformation of FLSYK on hGIIA (cyan) interacts with the region of the protein that is clearly different from the space occupied by the FLSYK ligand found in the 1JQ9 svPLA2 crystal structure (orange) (B). Also the overall conformations of these two ligands differ significantly. The best scoring docked FLSYK pose forms five hydrogen bonds denoted by yellow dashed lines formed between the ligand and the protein, at positions between a hydrogen of the N-terminus and the N δ 1 of His47, the oxygen of the backbone phenyl and the hydrogen of the backbone nitrogen of Gly29, the oxygen of the backbone serine and the hydrogen of the backbone nitrogen of Gly31, a hydrogen of the amino group of the lysine sidechain and the carboxyl oxygen of Glu55 sidechain, and an oxygen of the C-terminus and a hydrogen of the amino group of the Lys62 sidechain. Both A and B are in similar orientation to Figure 1.

Fig. 8

119x144mm (300 x 300 DPI)